Polymeric nanoantibiotics based on two orthogonal binding motifs coalesce with bacterial matter

Esteban Bautista,[1] Eduardo Estrada,[1] Jacob Deyell,[2,3] Melody Sun,[1] Albert R. La Spada,[2,3] Seunghyun Sim[1, 4, 5 *]

[1] Department of Chemistry, University of California Irvine, Irvine, California 92697, United States

[2] Departments of Pathology & Laboratory Medicine, Neurology, Biological Chemistry, and Neurobiology & Behavior, University of California Irvine, Irvine, California 92697, United States

[3] UCI Center for Neurotherapeutics, University of California Irvine, Irvine, CA 92697, United States

[4] Department of Chemical and Biomolecular Engineering, University of California Irvine, Irvine, California 92697, United States

[5] Department of Biomedical Engineering, University of California Irvine, Irvine, California 92697, United States

KEYWORDS: antimicrobial polymers & nanomedicine

ABSTRACT: Addressing the growing concern of antibiotic-resistant bacteria, we developed a series of novel polymeric nanoantibiotics with a dual-warhead system that induces physical lysis upon copolymer coalescence with bacterial matter. These polymers are equipped with two orthogonal binding motifs that form electrostatic interactions and dynamic covalent complexes on bacterial surfaces and exhibit potent antibacterial activity against gram-positive and gram-negative bacteria. The effect of the chemical composition and architecture of copolymers incorporating phenylboronic acid and quarternary ammonium groups on the antimicrobial activities was systematically examined. This work expands the current chemical repertoire to combat antimicrobial resistance by polymeric nanoantibiotics with a unique mode of action.

Introduction

Bacterial antimicrobial resistance (AMR) allows pathogens to tolerate and survive antibiotic treatment.[1, 2] AMR spontaneously occurs through the Darwinian selection process: Under the selective pressure of antibiotic exposure, microorganisms with newly acquired mutations of resistance genes will survive and proliferate.[3] In addition to random mutations, genetic materials encoding resistance genes can be exchanged between organisms.[4, 5] AMR is a growing concern in healthcare and agriculture and can lead to the next global health crisis.[6, 7] If the trend of AMR-associated illnesses continues, 10 million people could die annually by 2050.[8] It has been predicted that the massive use of antibiotics for the (co)treatment of COVID-19 will further exacerbate the ongoing AMR crisis in the future.[9, 10] Despite the sharply increasing trend of AMR, the pace of discovery and development of new antibiotics has been slow.[11] Only a few new classes of antibiotics are currently in the clinical

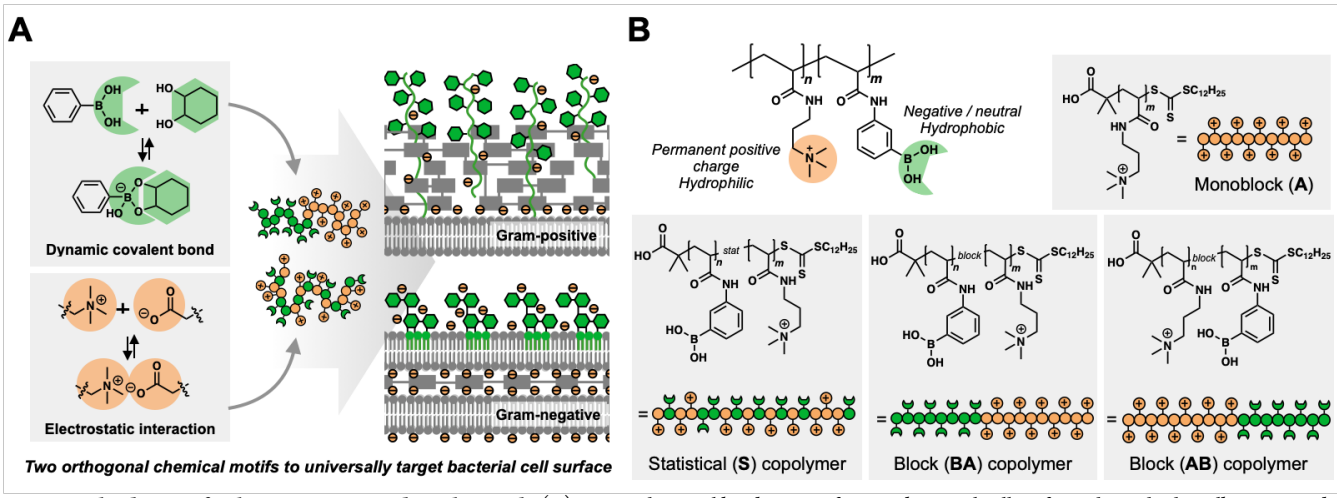

Figure 1. The design of polymeric compounds in this work. (A) Two orthogonal binding motifs target bacterial cell surfaces through phenylboronic acids and quaternary ammonium functional groups. Bacterial surface glycans with 1,2- and 1,3-diols are targeted with phenylboronic acids to form reversible dynamic covalent bonds. Quaternary ammonium groups target negatively charged bacterial surfaces through electrostatic interactions, specifically phosphoryl and carboxylate groups in lipopolysaccharides and teichoic acids in gram-negative and gram-positive bacteria, respectively. (B) Chemical structures of (co)polymers in this study.

development stage.[12] Therefore, there is an urgent need to develop antimicrobial agents with a new mode of action.

Synthetic antimicrobial polymers bring unique advantages in combating AMR. Advances in modern synthetic polymer chemistry have enabled precise control of the sequence and composition of polymeric species.[13] As such, incorporating key motifs from natural antibacterial compounds into synthetic polymeric species of controlled molecular weights and dispersity is possible.[14-18] Polymers can also mimic biological multivalent binding processes that create stronger binding than the sum of individual weak interactions.[19, 20] Another key feature of polymer-based antibiotic reagents, distinct from conventional small-molecule-based ones, is the scalability. Studies have reported the development of synthetic polymers or macromolecules with intrinsic antimicrobial activities by combining cationic motifs that target the negatively charged bacterial cell surface and hydrophobic portions that target and disrupt the cell membrane.[18, 21, 22] The effect of cationic and hydrophobic groups, their relative ratio, sequence, and topology have been investigated to enrich the repertoire of antimicrobial polymers, but more work needs to be done to expand the molecular scope, increase the efficacy, and develop a new mode of action unique to nanoscale polymeric agents.

Bacterial cell surfaces are complex environments that hold a variety of targetable handles. Gram-positive bacteria have a plasma membrane, which is covered with a thick peptidoglycan wall decorated with teichoic acids (Figure 1A).[23, 24] Gram-negative bacteria possess a double membrane structure – inner membrane and outer membrane, which contains surface-exposed lipopolysaccharides (Figure 1A). Between these two membranes, there is a thinner layer of peptidoglycan.[25, 26] In both gram species lay an abundance of negatively charged anions such as carboxylates and phosphoryl groups that provide both gram-positive and gram-negative cells with their characteristic negative surface charge (Figure 1A).[24-27] Primary amine and guanidium are popular choices as positively-charged cationic motifs due to their structural similarity with natural amino acids, lysine and arginine, respectively.[28-30] We have previously established that phenylboronic acids (PBA) form dynamic covalent bonds with surface-exposed diol species in bacteria and have utilized them as a chemical handle to assemble living materials.[31-33] Although there are a few reports describing the usage of PBA in developing antibacterial agents,[34, 35] to the best of our knowledge, PBA has not yet been systematically explored in the context of designing intrinsic antibacterial activities in polymer systems.

In this paper, we present the design, synthesis, and assessment of polymeric nanoantibiotics with a dual-warhead system that incorporates two orthogonal binding motifs to bacterial surfaces (Figure 1B). We sought to investigate whether the combination of PBA, which forms dynamic covalent bonds with available surface diols on the bacterial cell surface, and cationic residues in a single polymer chain yields antimicrobial polymers and how the composition and architecture of copolymers affect the antimicrobial activities. Because available lone pair electrons from an adjacent nitrogen can associate with the empty p orbital of PBA and potentially alter the diol-binding affinity,[36] we chose to harness quaternary ammonium as a permanently charged, orthogonal cationic motif that is expected to interact with negatively charged bacterial surfaces through electrostatic interactions. Strikingly, amphiphilic copolymers presented in our study undergo coalescence with bacterial matter, inducing physical lysis of bacterial cells.

RESULTS AND DISCUSSION

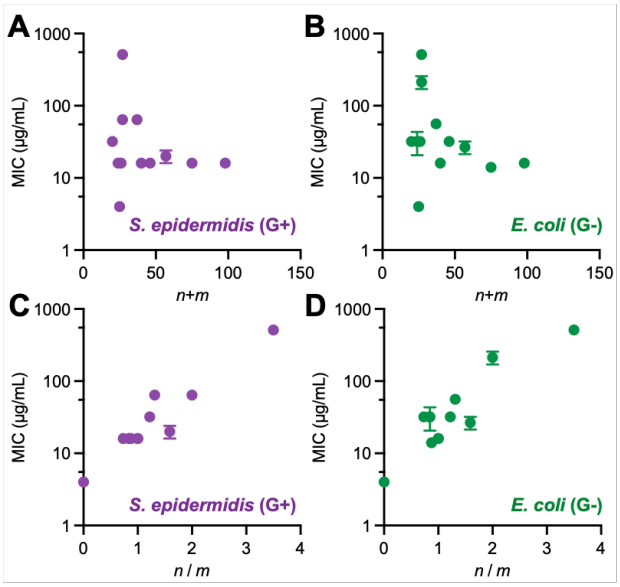

Figure 2. Screening of polymer library via MIC studies. (A–D) Copolymers of APTAC (*n* repeating unit) and APBA (*m* repeating unit) were tested against model gram-positive and negative strains, *S. epidermidis* (ATCC 12228) and *E. coli* (DH10B), respectively, in NB media. MIC values for (A) *S. epidermidis* and (B) *E. coli* are plotted as a function $n + m$. MIC values for (C) *S. epidermidis* and (D) *E. coli* are plotted as a function n/m. The MIC was defined as the lowest concentration that completely inhibited bacterial growth. Experiments were conducted in a biological quadruplicate ($N = 4$). Error bars correspond to standard error of mean (SEM).

Copolymer library reveals the effect of phenylboronic acid on antibacterial activity

A polymer library consisting of APBA (3-(acrylamido)phenylboronic acid) and APTAC (3-acrylamidopropyl)trimethylammonium) was synthesized via reversible addition-fragmentation chain transfer (RAFT) polymerization. This living radical polymerization allowed for the facile synthesis of well-defined polymers with varying degrees of polymerization, architectures, and end-group fidelity.[13, 37] 2-(dodecylthiocarbonothioylthio)-2-methylpropionic acid (DDMAT) was chosen as the CTA to synthesize a library of amphiphilic block copolymers. To begin understanding the structure-property relationship of BCPs bearing APBA and APTAC residues, four types of linear polymers were synthesized and characterized (Figure 1B, Figures S1–S19). Number average molecular weight (M_n) was determined via ^{1}H NMR by end-group analysis,[38] while weight-average molecular weight (M_w) was determined by diffusion-ordered spectroscopy (DOSY) NMR using a method reported by Junkers and coworkers (Supplementary Table 1).[39] Gel permeation chromatography (GPC) based characterization was not possible due to the adherent nature of these polymers.

After synthesizing a library of amphiphilic block copolymers, polymers of varying degrees of polymerization (DP) and architectures were evaluated for their antimicrobial activity via minimum inhibitory concentration (MIC) studies against a model gram-positive bacteria *Staphylococcus epidermidis* and gram-negative bacteria *Escherichia coli* (Figure 2). Antibacterial activities were examined as a function of the total number of repeating units ($n + m$) and the ratio of APBA to APTAC (n/m) based on NMR end-group analysis (Figure 2). Concerning the total number of repeating units ($n + m$), which also corresponds to polymer molecular weights against *S.*

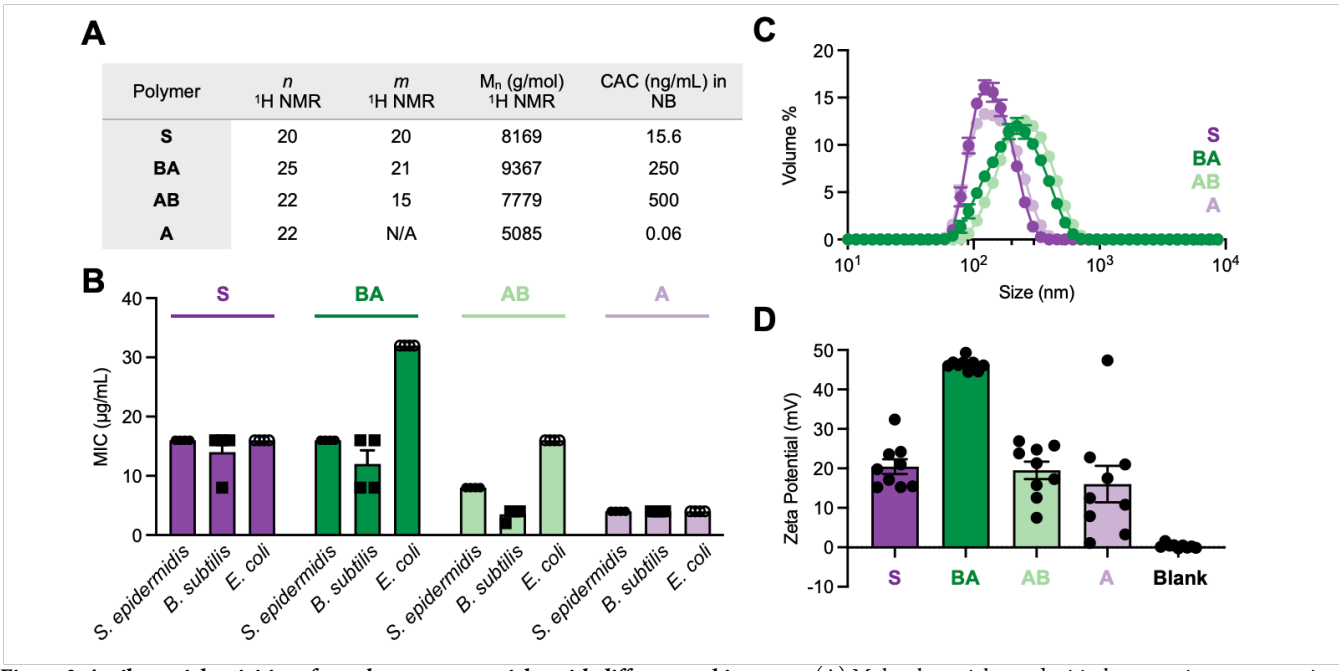

Polymer	*n* ^{1}H NMR	*m* ^{1}H NMR	M_n (g/mol) ^{1}H NMR	CAC (ng/mL) in NB
S	20	20	8169	15.6
BA	25	21	9367	250
AB	22	15	7779	500
A	22	N/A	5085	0.06

Figure 3. Antibacterial activities of copolymer nanoparticles with different architectures. (A) Molecular weights and critical aggregation concentration (CAC) of the selected polymers with similar compositions. The degrees of polymerization (*n* and *m*) and M_n were determined via ^{1}H NMR end-group analysis, and CAC values were determined by dynamic light scattering of diluted polymer solutions in NB media. (B) Comparison of antimicrobial activity in the selected polymers with similar compositions and different polymer architectures. Antimicrobial polymers were tested against *S. epidermidis* (ATCC 12228) *B. subtilis* (PY79), and *E. coli* (DH10B). (C) Dynamic light scattering (DLS) of antimicrobial polymers in NB media. (D) Zeta potential measurements of S, BA, AB, and A solutions in H_2O.

epidermidis, observed MICs did not have a clear trend (Figure 2A). For example, amphiphilic antimicrobial block copolymers of similar lengths, approximately 25 units, had significantly different MIC values, from as low as 4 μg/mL to as high as 512 μg/mL. A similar relationship was found in *E. coli* (Figure 2B). Next, the relationships between the amount of APBA and APTAC and antimicrobial activity were investigated. Increasing APTAC (*n*) in copolymers generally decreased the MICs (Figure S21), whereas there was no clear trend between the amount of APBA (m) and MICs (Figure S21). In both strains, as the ratio of APBA to APTAC increased, antimicrobial activity decreased (Figures 2C and 2B). A polymer without an APBA unit (*n*/*m* ratio of 0) resulted in a MIC of 4 μg/mL, and by increasing the percentage of APBA in copolymer chains, higher MIC values are observed. It directly shows that incorporating APBA in copolymers attenuates the antibacterial activity of permanently charged amphiphilic cationic polymers. We speculate that the interaction of APBA with surface-exposed diols (e.g., teichoic acids) limits the penetration of copolymers into the cell membrane.

Antibacterial activity of polymer nanoparticles

Having established the effect of copolymer composition in antibacterial activities, we sought to gain a deeper understanding of the structure-property relationship and mode of antibacterial activities of these copolymers. We selected copolymers with comparable molecular weights and different polymer architectures, statistical copolymer (S), and diblock copolymers (AB and BA) based on the sequence (Figure 1B) for detailed comparison. We also prepared a monoblock polymer with only APTAC (A) for comparison, along with a monoblock polymer of APBA (B) that was insoluble in water. Further, polymers S and BA were cleaved of their CTA and tested for antibacterial activities. The critical aggregation concentration (CAC) of these polymers was determined in NB media,[40] where we performed all of our MIC experiments (Figure 1B). Polymers S and A with statistical and monoblock architectures had the lowest CAC values at 15.6 and 0.06 ng/mL, while polymers BA and AB with block architectures had the highest CACs at 250 and 500 ng/mL, respectively (Figure 3A and Figure S20).

All polymers (S, BA, AB, and A) demonstrated potent antibacterial activity against gram-positive bacteria *S. epidermidis* and *Bacillus subtilis* and gram-negative bacteria *E. coli* (Figure 3B). In all of the tested bacterial strains, polymer A showed the most potent antimicrobial activity. The second most effective polymer was AB, with its highest observed MIC value being 16 μg/mL against *E. coli* and its lowest being 3.5 μg/mL against *B. subtilis*. The other diblock copolymer BA showed slightly higher MIC values across all three strains. The CTA-removed version of S showed a two-fold increase in MIC values in *S. epidermidis* and *E. coli* when compared to polymer S, whereas polymer BA without a CTA produced almost identical MIC values to polymer BA (Supplementary Table 2). Considering the relatively similar values of MICs in these CTA-removed copolymers, membrane disruption for polymers S and BA does not seem to rely on the dodecyl functional group of the CTA. Because these MIC values are well above the CAC values of the polymers, we investigated the hydrodynamic sizes of the self-assembled polymers at MIC. Dynamic light scattering (DLS) measurements revealed the average hydrodynamic radii (R_h) for assembled polymers in the range of hundreds of nanometers, with S and A being slightly smaller than block copolymers BA and AB, at concentrations around MIC of the three bacterial cell lines (Figure 3C). The amphiphilic nature of these polymers, which comprise a hydrophilic portion of the permanently charged cationic residues and a hydrophobic portion of

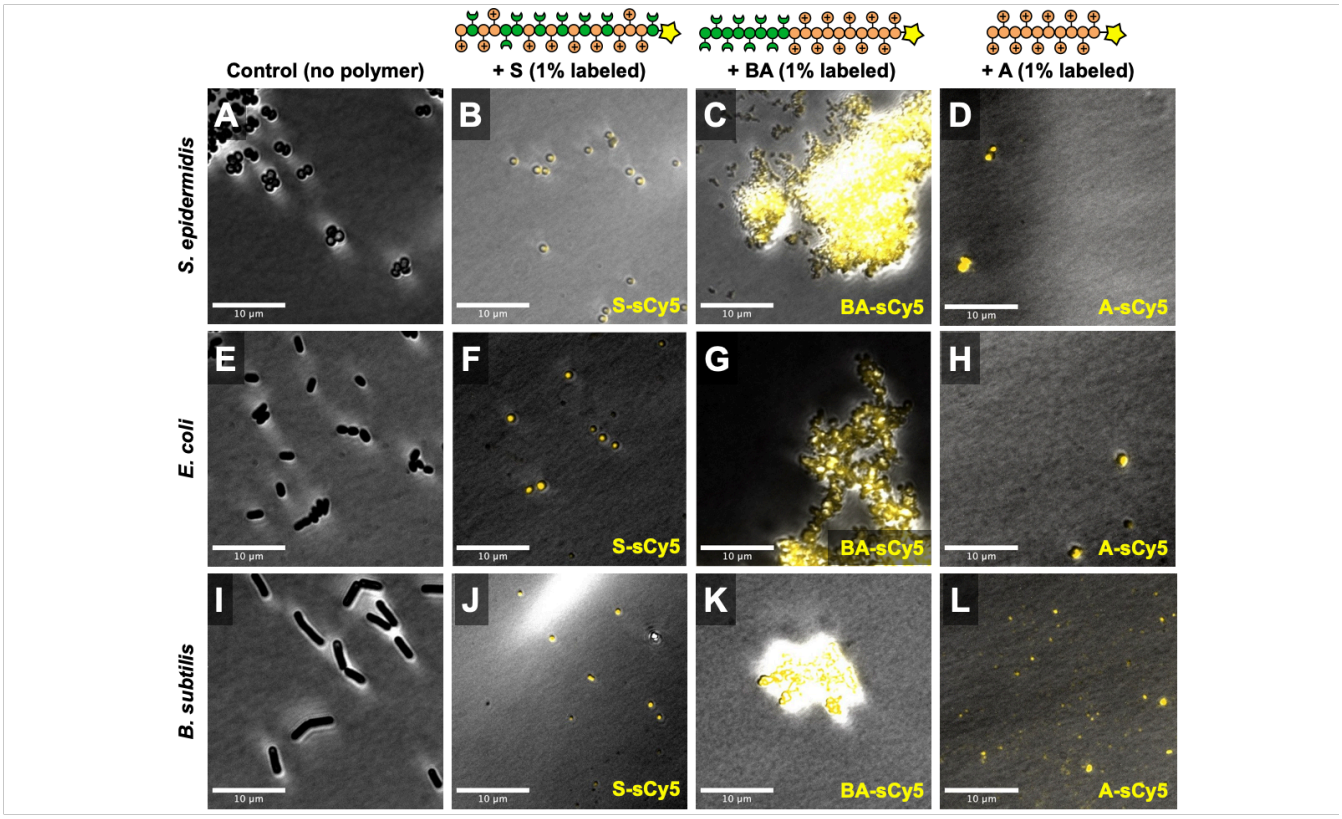

Figure 4. Tracking nanoantibiotic polymers' mode of action. Polymers BA, S, and A were conjugated with sCy5 fluorophore for *in situ* polymer tracking after treating cells. Polymer solutions containing 1% of sCy5-conjugated polymers were prepared at their respective MIC concentrations. Fluorescence images (λ_{ex} = 630 nm, λ_{obs} = 690–740 nm) were taken after treating *S. epidermidis*, *E. coli*, or *B. subtilis* with polymer solutions for 16-h at 37 °C and 250 RPM. (A) *S. epidermidis* without polymer treatment. (B) *S. epidermidis* incubated with S (1% S-sCy5) (C) *S. epidermidis* incubated with BA (1% BA-sCy5). (D) *S. epidermidis* incubated with A (1% A-sCy5). (E) *E. coli* without polymer treatment. (F) *E. coli* incubated with S (1% S-sCy5) (G) *E. coli* incubated with BA (1% BA-sCy5). (H) *E. coli* incubated with A (1% A-sCy5). (I) *B. subtilis* without polymer treatment. (J) *B. subtilis* incubated with S (1% S-sCy5) (K) *B. subtilis* incubated with BA (1% BA-sCy5). (L) *B. subtilis* incubated with A (1% A-sCy5). Scale bars = 10 μm.

the dodecyl chain and phenylboronic acid residues, drives the assembly of polymer micelles in the nanoscale (Figure S20). Zeta potential measurements were also performed for these polymers at their highest observed MICs. They all showed positive values due to the permanently charged APTAC units (Figure 3D). Considering that copolymers S, AB, and BA showed similar or larger zeta potential values, the incorporation of APBA does not lead to a decrease in positive surface charge in physiological conditions.

Physical lysis of bacterial cells by polymer nanoparticles

The general mode of action for antibacterial agents can be classified into two categories: bacteriostatic agents that arrest the growth of cells and bactericidal agents that cause cell death.[41] We sought to investigate the mode of action for antimicrobial polymers by synthesizing fluorescently labeled polymeric probes (S2.4.1.–S2.4.3.). Briefly, they were synthesized by cleaving dodecyl groups to produce terminal thiols, followed by a subsequent reaction with sulfo-cyanine5 (sCy5) maleimide. Fluorescent probes (S-sCy5, BA-sCy5, and A-sCy5) were mixed (1%) with their nonfluoregenic counterpart and exposed to bacteria at their MIC to track the localization of polymers (Figure 4). Cells treated with S-sCy5 all showed fluorogenic spherical microstructures (Figures 4B, 4F, and 4J). These structures are evidently different in dimensions from intact, rod-shaped *E. coli* or *B. subtilis* cells (Figures 4E–F and 4I–J). In the case of *S. epidermidis*, these microstructures have a similar spherical shape but slightly smaller dimensions (Figure 4A–B). Notably, the size of these microstructures is much bigger than polymer S in solutions (Figure 3C), suggesting the possible coassembly of S with bacterial cellular matter from lysed cells or physically deformed cells penetrated by S. On the other hand, cells treated with BA-sCy5 all lost their intact structures and dimensions, and large fluorogenic aggregates emerged (Figures 4C, 4G, and 4K). The size of the self-assembled structures of BA increased from hundreds of nanometers (Figure 3C) to tens of micrometer-scale assemblies. We speculate that bound BA on the cell surface and their subsequent aggregation is the physical cause for the observed cell lysis. Cells treated with A also lost their physical structures, and fluorescent microstructures of various sizes and shapes were observed instead (Figures 4D, 4H, and 4L). In all cases, we observed the loss of physical features of intact cells and the emergence of fluorescent microstructures, indicating that these polymers physically lyse and kill bacterial cells at concentrations higher than MIC.

To fully demonstrate that these polymers physically lyse bacterial cells, we employed engineered *B. subtilis*, which constitutively expresses cytosolic red fluorescence protein (RFP). Upon cell lysis, the intracellular RFP leaks out to the supernatant (Figure 5A). Cells

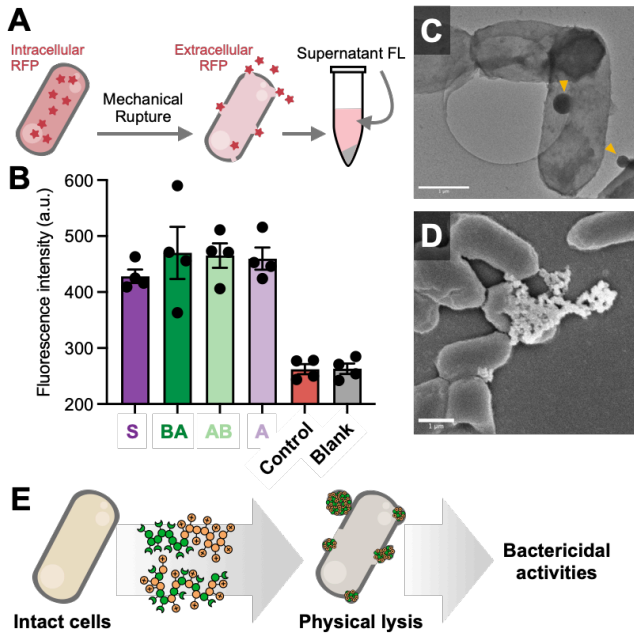

Figure 5. Physical lysis of bacterial cells upon treatment with polymeric nanoantibiotics. (A) Schematic illustration of the cell lysis test with *B. subtilis* expressing cytosolic red fluorescent protein (RFP). Physical lysis of cells would lead to RFP leakage in the supernatant. (B) Fluorescence intensity measurements of RFP (excitation = 550 nm, emission = 585 nm) in the supernatant after cells were incubated at their respective MIC for 16-h at 37 °C and 250 RPM in quadruplicate. (C) Cryo-TEM image of *E. coli* treated with S at 8 μg/mL (0.5 MIC). (D) SEM image of *E. coli* treated with polymer AB at 8 μg/mL (0.5 MIC). Scale bars = 1 μm. (E) Bactericidal activities of polymers in this study arise from cell surface binding and coalescence with bacterial matter.

treated with S, BA, AB, and A at their MIC all showed a significant increase in RFP emission in the supernatant, corroborating that these polymers induce physical lysis of cells and that their mode of action is bactericidal (Figure 5B). We also imaged *S. epidermidis* and *E. coli* after treatment with antimicrobial polymers using electron microscopy to gain structural insights for microstructures observed in fluorescence studies (Figure 5). We note that the cells in these images were treated with half of the MIC to observe any intermediate feature forming with or on cells. When cells were treated with polymers at MIC, we were not able to find any cellular structures. Cryogenic transmission electron microscopy (cryo-TEM) revealed a spherical microstructure forming on *E. coli* treated with S (Figures 5C and S22). These images also show that S induces deformation of the cell surface, pore formation, and cell leakage, eventually leading to the complete physical lysis of cells (Figure S22). We attribute it to the synergistic effect of binding to the cell surface and the tendency of polymers to assemble from their amphiphilic designs. Aggregates formed after treating BA and AB were observed by scanning electron microscopy (SEM) (Figures 5D and S23). They were primarily observed on deformed cell surfaces, showing that the binding and self-assembling behavior induces physical rupture of bacterial cells. Upon exposure to A, cells exhibited significant changes in their surface topology, including membrane disruption and pore formation (Figure S23). Altogether, these amphiphilic polymers act by binding to the cell surface and coalescing with the cellular components, leading to the physical lysis of bacterial cells (Figure 5E). Changing polymer architectures granted access to different microscopic morphologies as a result of their bactericidal activities (Figure 4).

Biocompatibility of polymeric nanoantibiotics

Polymeric nanoantibiotics were assessed for their cytocompatibility via cytotoxicity studies against human embryonic kidney cells (HEK 293). These polymers are generally not toxic to HEK 293 at concentrations toxic to bacterial cells (Figure 6A). Block copolymers BA and AB were found to be slightly more toxic to HEK 293 than S or A, based on the cell viability at higher concentrations (Figure S24). We speculate that the selectivity toward bacteria over mammalian cells is accomplished by a greater negative surface charge of bacteria than mammalian cells.[42, 43] Hemocompatibility was evaluated via hemolysis and hemagglutination assays against sheep red blood cells (RBC). These polymers are generally hemolytic at high concentrations but not at or near their respective MICs (Figures 6A and S25). Polymers S, BA, and AB induced aggregation of sheep RBCs at concentrations below their MICs at 8, 2, and 4 μg/mL, respectively (Figures 6A–E). We reasoned that the formation of dynamic covalent bonds of APBA with RBC surface glycans is likely the cause of this phenomenon. Cleaving the CTAs of S and BA did not improve or reduce their biocompatibility across the cytotoxicity, hemolysis, or hemagglutination assays (S24 - S25, and Supplementary Table 3). Despite poor hemocompatibility with antimicrobial polymers inducing RBC aggregation, these polymers demonstrate cytocompatibility.

CONCLUSIONS

AMR is projected to worsen with time, and the toolbox to eradicate antibiotic-resistant bacteria needs to be expanded to include novel design principles and modes of action. In this work, we presented the design, synthesis, and evaluation of polymeric nanoantibiotics with a dual-warhead system that incorporates two orthogonal binding motifs. To the best of our knowledge, our work provides an

A

Polymer	Cytotoxicity (IC_{50}) (μg/mL) HEK 293	Hemolysis (IC_{50}) (μg/mL)	Hemagglutination (C_H) (μg/mL)
S	> 512	> 512	8
BA	> 512	> 512	2
A	> 512	> 512	512
AB	> 512	512	4

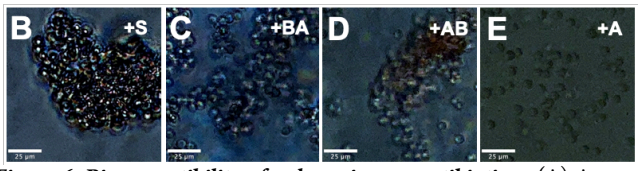

Figure 6. Biocompatibility of polymeric nanoantibiotics. (A) A summary table of biocompatibility based on cytotoxic, hemolytic, and hemagglutination activity of polymeric nanoantibiotics. Cytotoxicity (IC_{50}) is the minimum concentration of nanoantibiotic needed for 50% cell viability of Human Embryonic Kidney (HEK) 293 cells. Hemolysis (IC_{50}) is the minimum concentration of nanoantibiotic needed for 50% lysis of RBCs. Hemagglutination (C_H) is determined by the minimum concentration of nanoantibiotic needed for 10% aggregation of RBCs. Assays were conducted in quadruplicate. (B–E) Optical microscopy images of RBCs upon exposure to (B) S, (C) BA, (D) AB, (E) A. Images were taken at respective C_H for each polymer. Scale bars = 25 μm.

example of systematically examining the effect of phenylboronic acid in cationic copolymers, both in composition and architecture. From the MIC analysis of polymer library varying compositions, we found that increasing the portion of phenylboronic acid in copolymers leads to decreased antimicrobial activity. Our work also establishes that these copolymers are bactericidal by physically lysing the cells and coalescing with bacterial matter. Selected polymers with different architecture and similar chemical compositions showed that the architecture determines the morphology and size of the structures formed by polymer and bacterial matter.

These polymeric agents have important implications for the next generation of AMR treatments since they do not require separate loading of antibiotics and work in both gram species. Future work in this area involves further expanding the chemical scope and accessing antibiotic-resistant bacteria. This work pushes the limits on the nanoscale self-assembly that can be achieved on the surface of bacteria and lays down design cues for future antibacterial agents.

METHODS

DOSY (Diffusion-Ordered Spectroscopy) NMR. Weight averaged molecular weight (M_w) was calculated using an established protocol.[39] Briefly, polymer stock solutions were prepared in D_2O at 1 mg/mL concentrations to obtain diffusion coefficients. Once obtained, M_w was calculated as follows: $\log(D) + \log(\eta) = \log(c) + \nu\log(M)$. D = diffusion coefficient, η = viscosity of D_2O, c = 1st calibration coefficient for PEG in D_2O, ν = 2nd calibration coefficient for PEG in D_2O.

Dynamic Light Scattering (DLS). Polymer stock solutions were prepared in NB media, and aliquots of the stock solutions were diluted to desired concentrations (0.03 ng/mL – 32 μg/mL, except polymer A (final concentration = 16 μg/mL). Polymer solutions were then placed on a heating block (37 °C at 250 RPM) overnight, and DLS measurements were taken the next day at room temperature with a 90° scattering detector angle for size measurements. The critical aggregation concentration (CAC) was determined by plotting the average R_h as a function of polymer concentration and by applying a simple linear regression with the CAC being the inflection point.

Minimum Inhibitory Concentration (MIC). Polymeric nanoantibiotics were evaluated for their antimicrobial activity using established protocols.[44] Briefly, stock solutions of the antimicrobial polymers were created in NB media and then diluted in 96-well plates with 2-fold dilutions from 512 μg/mL to 1 μg/mL. Bacteria were grown (37 °C, 250 rpm) to a 1 x 10^8 CFU/mL to match the McFarland 0.5 standard. Bacterial suspensions were diluted 100-fold, and then 50 µL of the bacterial suspensions were added to the 96-well plate, creating a final inoculum size of 5 x 10^5 CFU/mL. Bacterial growth was determined after 16 hours of incubation at 37 °C by optical density (OD_{600}) using a BioTek™ Synergy™ H1 Hybrid Multi-Mode microplate reader. The MIC was defined as the lowest concentration that completely inhibited bacterial growth (no increase in OD). Each experiment was conducted in biological quadruplicates per combination of bacterial strain, polymer, and concentration.

Zeta Potential. Polymer stock solutions were prepared in doubly distilled H_2O, and aliquots of the stock solutions were diluted to the desired concentrations – the highest MIC observed across all bacterial cell lines. Samples were then placed on a heating block overnight (37 °C at 250 RPM), and zeta potential measurements were performed at room temperature in triplicates.

In situ polymer tracking via sCy5 conjugated polymers. sCy5 localization experiments were conducted similarly to MIC studies. Briefly, stock solutions of the antimicrobial polymers were created in NB media, and their sCy5 conjugate was added to create a 1% sCy5 conjugated polymer solution, with 99% being unmodified polymer. Aliquots were then diluted in 96-well plates via 2-fold dilutions from 512 μg/mL to 1 μg/mL. Bacterial suspensions were added to the 96-well plate, creating a final inoculum size of 5 x 10^5 CFU/mL. Fluorescent images were taken at the concentration that completely inhibited bacterial growth (no increase in OD). Experiments were conducted in quadruplicate for each combination of bacterial strain, polymer, and concentration. Fluorescent microscopy images were taken for each sample (λ_{ex} = 630 nm, λ_{obs} = 690–740 nm).

RFP intensity measurements. The fluorescent intensity of RFP in the supernatant was measured after antimicrobial polymer exposure against RFP-expressing *B. subtilis*. Briefly, polymer stock solutions were created in NB media and then diluted in 96-well plates with 2-fold dilutions from 512 μg/mL to 1 μg/mL. RFP-expressing *B. subtilis* was grown to an OD_{600} = 1.0 (37 °C, 250 rpm) and was added into a 96-well plate. Bacterial growth was determined after 16 hours of incubation at 37 °C by OD_{600}. The lowest concentration that completely inhibited bacterial growth was centrifuged at 5000 RPM for 10 minutes. 100 µL of the supernatant was carefully transferred to a new plate, and fluorescent intensity measurements were done using a BioTek™ Synergy™ H1 Hybrid Multi-Mode microplate reader (λ_{ex} = 558 nm, λ_{em} = 580 nm). Fluorescent microscopy imaging was accomplished using an RVL-100-M model ECHO Revolve fluorescence microscope at 60x magnification with a phase-contrast objective (λ_{ex} = 530 nm, λ_{obs} = 605–670 nm). Each experiment was conducted in quadruplicate per combination of polymer and concentration.

Cryo-TEM. Before sample deposition, TEM grids were treated for glow discharge to hydrophilize the support film for ~ 90 seconds. Next, 5 μL of sample (at half the MIC) was deposited onto the TEM grid and was allowed to sit for 10 minutes. The grid was washed with 200 μL of doubly distilled H_2O and then blotted dry with filter paper. Once dried 5 μL of 2% uranyl acetate was deposited onto the grid for 15 seconds and then blotted dry with filter paper. TEM imaging was performed using a JEOL JEM-2100F TEM equipped with a Schottky-type field emission electron source at an accelerating voltage of 200 kV. Images were taken using a Gatan Oneview camera.

SEM. Interactions between polymeric nanoantibiotics and bacteria were taken using an established protocol.[45] Briefly, samples at half the MIC were concentrated at 5000 RPM for 10 minutes. The media was discarded, and the cell pellet was resuspended in 4.0% glutaraldehyde solution (in 1x PBS) for 1 hour. Next, a glass cover slide was precoated with poly-D-lysine (50 μg/mL in H_2O) for 15 minutes, and the excess was removed with doubly distilled H_2O. After the sample was fixed for 1 hour, 30 μL was deposited onto the glass slide for 15 minutes and then washed with doubly distilled H_2O. The sample/glass slide was treated with ethanol solutions (30%, 50%, 70%, 90%, and 100% in doubly distilled H_2O) for 10 minutes each. The samples were air-dried and sputter-coated with iridium. SEM was performed on a Tescan GAIA3 SEM-FIB equipped with a field emission gun at an operating voltage of 4 kV and an in-beam SE detector.

Cytotoxicity Assay. Cytotoxic activity of polymeric nanoantibiotics was evaluated using established protocols.[21, 46] Briefly, HEK-293T cells were plated in a 96-well plate at a density of 4,000 cells/well and left to settle overnight. Cells were cultured in DMEM + GlutaMAX. The following day, cells were treated with varying concentrations of the polymer dissolved in media, with blank media being used as a negative control. After 24 hours of treatment with the polymer, 10 μL of Presto Blue was added to the cells and was left to incubate for 3 hours. Absorbance readings at 570 nm were taken for the plate after that time using a Varioskan LUX

Multimode Microplate Reader. Cell viability was expressed as a percentage relative to the cells that were treated with blank media.

Hemolysis. Hemolytic activity of polymeric nanoantibiotics was evaluated using established protocols.[15,21] Defibrinated sheep blood was centrifuged at 4500 g for 1 minute with subsequent washes with 1x PBS until the supernatant of the blood was clear, at which point the RBCs were resuspended at 6% (v/v). 100 μL of the RBCs were added to each well of a 96-well plate. 100 μL of the polymer solution was added to each well to reach the desired concentration. 1x PBS was used as a negative control for hemolysis, while 1% Triton X-100 was used as a positive hemolytic control. After the polymer was added to the RBCs, the plate was incubated at 37 °C for 2 hours, after which time the plate was centrifuged at 600 g for 10 minutes. 100 μL of the supernatant was carefully withdrawn and transferred to a new plate. Absorbance readings at 540 nm were measured using a Varioskan LUX Multimode Microplate Reader. Readings were normalized to the Triton X-100 group, which was considered 100% hemolysis. The percentage of hemolysis was calculated as follows: % Hemolysis = [(sample absorbance – negative control) / (positive control – negative control)] ×100%.

Hemagglutination. Hemagglutination assays were performed using established protocols.[15,21] Sheep RBCs were prepared as described above. 50 μL of the 6% (v/v) RBCs were added to each test well of a 96-well U-bottom plate, followed by 50 μL of polymer at the specified concentration. 0.05 mg/mL Concanavalin A was used as a positive control, and PBS was used as a negative control. The plates were incubated at 37 °C for 1 hour, after which time the plates were visually assessed for hemagglutination. Images were captured for each well. Representative microscopy images of several conditions were also taken to demonstrate the hemagglutination.

ASSOCIATED CONTENT

Supporting Information

The Supporting Information is available free of charge on the ACS Publications website.

Materials, instrumentations, experimental and synthetic methods, ^{1}H and DOSY NMR spectra, CAC plots, fluorescence microscopy, TEM, and SEM images, cytotoxicity, hemolysis, and hemagglutination data (PDF).

AUTHOR INFORMATION

Corresponding Author

* **Seunghyun Sim** –Department of Chemistry, Department of Biomedical Engineering, Department of Chemical and Biomolecular Engineering, University of California, Irvine, California 92697; Center for Complex and Active Materials, University of California, Irvine, Irvine, California 92697, United States;
Email: s.sim@uci.edu

Author Contributions

The manuscript was written through contributions of all authors, and all authors have given approval to the final version of the manuscript.

ACKNOWLEDGMENT

This work is supported by the UC Irvine start-up fund and by the National Institute of General Medical Sciences of the National Institutes of Health under Award Numbers R35GM150770 and R35NS122140. The content is solely the responsibility of the authors and does not necessarily represent the official views of the National Institutes of Health. E. B. acknowledges support from the National Science Foundation Graduate Research Fellowship Program (DGE-1839285). E. E. was supported by UROP fellowship from UC Irvine, and J. D. was supported by F30 Award F30AG081084. The authors acknowledge the use of facilities and instrumentation at the UC Irvine Materials Research Institute (IMRI) supported in part by the National Science Foundation Materials Research Science and Engineering Center program through the UC Irvine Center for Complex and Active Materials (DMR-2011967). Dynamic light scattering and zeta potential measurements were performed at the Laser Spectroscopy Labs, and the Nuclear Magnetic Resonance measurements were done in the NMR facility, both in the Department of Chemistry, University of California, Irvine.

REFERENCES

(1) Brauner, A.; Fridman, O.; Gefen, O.; Balaban, N. Q. Distinguishing between resistance, tolerance and persistence to antibiotic treatment. *Nature Reviews Microbiology* **2016**, *14*(5), 320-330.
(2) Kapoor, G.; Saigal, S.; Elongavan, A. Action and resistance mechanisms of antibiotics: A guide for clinicians. *Journal of Anaesthesiology Clinical Pharmacology* **2017**, *33*(3), 300-305.
(3) Holmes, A. H.; Moore, L. S. P.; Sundsfjord, A.; Steinbakk, M.; Regmi, S.; Karkey, A.; Guerin, P. J.; Piddock, L. J. V. Understanding the mechanisms and drivers of antimicrobial resistance. *The Lancet* **2016**, *387*(10014), 176-187.
(4) Soucy, S. M.; Huang, J.; Gogarten, J. P. Horizontal gene transfer: building the web of life. *Nature Reviews Genetics* **2015**, *16*(8), 472-482.
(5) Arnold, B. J.; Huang, I. T.; Hanage, W. P. Horizontal gene transfer and adaptive evolution in bacteria. *Nature Reviews Microbiology* **2022**, *20*(4), 206-218.
(6) Chin, K. W.; Michelle Tiong, H. L.; Luang-In, V.; Ma, N. L. An overview of antibiotic and antibiotic resistance. *Environmental Advances* **2023**, *11*, 100331.
(7) Okeke, I. N.; de Kraker, M. E. A.; Van Boeckel, T. P.; Kumar, C. K.; Schmitt, H.; Gales, A. C.; Bertagnolio, S.; Sharland, M.; Laxminarayan, R. The scope of the antimicrobial resistance challenge. *The Lancet* **2024**, *403*(10442), 2426-2438.
(8) Murray, C. J. L.; Ikuta, K. S.; Sharara, F.; Swetschinski, L.; Robles Aguilar, G.; Gray, A.; Han, C.; Bisignano, C.; Rao, P.; Wool, E.; et al. Global burden of bacterial antimicrobial resistance in 2019: a systematic analysis. *The Lancet* **2022**, *399*(10325), 629-655.
(9) Rawson, T. M.; Ming, D.; Ahmad, R.; Moore, L. S.; Holmes, A. H. Antimicrobial use, drug-resistant infections and COVID-19. *Nature Reviews Microbiology* **2020**, *18*(8), 409-410.
(10) Hsu, J. How covid-19 is accelerating the threat of antimicrobial resistance. *Bmj* **2020**, *369*.
(11) Miethke, M.; Pieroni, M.; Weber, T.; Brönstrup, M.; Hammann, P.; Halby, L.; Arimondo, P. B.; Glaser, P.; Aigle, B.; Bode, H. B. Towards the sustainable discovery and development of new antibiotics. *Nature Reviews Chemistry* **2021**, *5*(10), 726-749.
(12) Butler, M. S.; Henderson, I. R.; Capon, R. J.; Blaskovich, M. A. T. Antibiotics in the clinical pipeline as of December 2022. *The Journal of Antibiotics* **2023**, *76*(8), 431-473.
(13) Perrier, S. 50th Anniversary Perspective: RAFT Polymerization—A User Guide. *Macromolecules* **2017**, *50*(19), 7433-7447.
(14) Parkin, H. C.; Street, S. T. G.; Gowen, B.; Da-Silva-Correa, L. H.; Hof, R.; Buckley, H. L.; Manners, I. Mechanism of Action and Design of Potent Antibacterial Block Copolymer Nanoparticles. *Journal of the American Chemical Society* **2024**, *146*(8), 5128-5141.
(15) Laroque, S.; Garcia Maset, R.; Hapeshi, A.; Burgevin, F.; Locock, K. E. S.; Perrier, S. Synthetic Star Nanoengineered Antimicrobial Polymers as

Antibiofilm Agents: Bacterial Membrane Disruption and Cell Aggregation. *Biomacromolecules* **2023**, *24*(7), 3073-3085.
(16) Lehnen, A.-C.; Bapolisi, A. M.; Krass, M.; AlSawaf, A.; Kurki, J.; Kersting, S.; Fuchs, H.; Hartlieb, M. Shape Matters: Highly Selective Antimicrobial Bottle Brush Copolymers via a One-Pot RAFT Polymerization Approach. *Biomacromolecules* **2022**, *23* (12), 5350-5360.
(17) Judzewitsch, P. R.; Nguyen, T. K.; Shanmugam, S.; Wong, E. H.; Boyer, C. Towards sequence-controlled antimicrobial polymers: effect of polymer block order on antimicrobial activity. *Angewandte Chemie International Edition* **2018**, *57*(17), 4559-4564.
(18) Pham, P.; Oliver, S.; Boyer, C. Design of antimicrobial polymers. *Macromolecular Chemistry and Physics* **2023**, *224*(3), 2200226.
(19) Ravnik, V.; Bren, U.; Curk, T. Designing Multivalent Copolymers for Selective Targeting of Multicomponent Surfaces. *Macromolecules* **2024**, *57*(13), 5991-6002.
(20) van Dongen, M. A.; Dougherty, C. A.; Banaszak Holl, M. M. Multivalent Polymers for Drug Delivery and Imaging: The Challenges of Conjugation. *Biomacromolecules* **2014**, *15*(9), 3215-3234.
(21) Salas-Ambrosio, P.; Vexler, S.; P S, R.; Chen, I. A.; Maynard, H. D. Caffeine and Cationic Copolymers with Antimicrobial Properties. *ACS Bio & Med Chem Au* **2023**, *3*(2), 189-200.
(22) Haktaniyan, M.; Bradley, M. Polymers showing intrinsic antimicrobial activity. *Chemical Society Reviews* **2022**, *51* (20), 8584-8611.
(23) Rohde, M. The Gram-Positive Bacterial Cell Wall. *Microbiology Spectrum* **2019**, *7*(3).
(24) Brown, S.; Santa Maria Jr, J. P.; Walker, S. Wall teichoic acids of gram-positive bacteria. *Annual review of microbiology* **2013**, *67*(1), 313-336.
(25) Beveridge Terry, J. Structures of Gram-Negative Cell Walls and Their Derived Membrane Vesicles. *Journal of Bacteriology* **1999**, *181* (16), 4725-4733.
(26) Silhavy, T. J.; Kahne, D.; Walker, S. The bacterial cell envelope. *Cold Spring Harbor perspectives in biology* **2010**, *2*(5), a000414.
(27) Wilson, W. W.; Wade, M. M.; Holman, S. C.; Champlin, F. R. Status of methods for assessing bacterial cell surface charge properties based on zeta potential measurements. *Journal of Microbiological Methods* **2001**, *43*(3), 153-164.
(28) Li, X.; Bai, H.; Yang, Y.; Yoon, J.; Wang, S.; Zhang, X. Supramolecular antibacterial materials for combatting antibiotic resistance. *Advanced Materials* **2019**, *31*(5), 1805092.
(29) Jain, A.; Duvvuri, L. S.; Farah, S.; Beyth, N.; Domb, A. J.; Khan, W. Antimicrobial polymers. *Advanced healthcare materials* **2014**, *3* (12), 1969-1985.
(30) Si, Z.; Zheng, W.; Prananty, D.; Li, J.; Koh, C. H.; Kang, E.-T.; Pethe, K.; Chan-Park, M. B. Polymers as advanced antibacterial and antibiofilm agents for direct and combination therapies. *Chemical Science* **2022**, *13* (2), 345-364.
(31) Jo, H.; Sim, S. Programmable Living Materials Constructed with the Dynamic Covalent Interface between Synthetic Polymers and Engineered B. subtilis. *ACS Applied Materials & Interfaces* **2022**, *14* (18), 20729-20738.
(32) Jo, H.; Selmani, S.; Guan, Z.; Sim, S. Sugar-Fueled Dissipative Living Materials. *Journal of the American Chemical Society* **2023**, *145*(3), 1811-1817.
(33) Kawada, M.; Jo, H.; Medina, A. M.; Sim, S. Catalytic Materials Enabled by a Programmable Assembly of Synthetic Polymers and Engineered Bacterial Spores. *Journal of the American Chemical Society* **2023**, *145*(29), 16210-16217.
(34) Wang, L.; Zheng, W.; Zhong, L.; Yang, Y.; Chen, Y.; Hou, Q.; Yu, P.; Jiang, X. Phenylboronic Acid-Modified Gold Nanoclusters as a Nanoantibiotic to Treat Vancomycin-Resistant Enterococcus faecalis-Caused Infections. *ACS Nano* **2023**, *17*(20), 19685-19695.
(35) Huang, F.; Cai, X.; Hou, X.; Zhang, Y.; Liu, J.; Yang, L.; Liu, Y.; Liu, J. A dynamic covalent polymeric antimicrobial for conquering drug-resistant bacterial infection. *Exploration* 2022; Wiley Online Library: Vol. 2, p 20210145.
(36) Bosch, L. I.; Fyles, T. M.; James, T. D. Binary and ternary phenylboronic acid complexes with saccharides and Lewis bases. *Tetrahedron* **2004**, *60*(49), 11175-11190.
(37) Semsarilar, M.; Abetz, V. Polymerizations by RAFT: Developments of the Technique and Its Application in the Synthesis of Tailored (Co) polymers. *Macromolecular Chemistry and Physics* **2021**, *222* (1), 2000311.
(38) Izunobi, J. U.; Higginbotham, C. L. Polymer Molecular Weight Analysis by 1H NMR Spectroscopy. *Journal of Chemical Education* **2011**, *88*(8), 1098-1104.
(39) Voorter, P. J.; McKay, A.; Dai, J.; Paravagna, O.; Cameron, N. R.; Junkers, T. Solvent-Independent Molecular Weight Determination of Polymers Based on a Truly Universal Calibration. *Angewandte Chemie International Edition* **2022**, *61*(5), e202114536.
(40) Topel, Ö.; Çakır, B. A.; Budama, L.; Hoda, N. Determination of critical micelle concentration of polybutadiene-block-poly(ethyleneoxide) diblock copolymer by fluorescence spectroscopy and dynamic light scattering. *Journal of Molecular Liquids* **2013**, *177*, 40-43.
(41) Pankey, G. A.; Sabath, L. D. Clinical Relevance of Bacteriostatic versus Bactericidal Mechanisms of Action in the Treatment of Gram-Positive Bacterial Infections. *Clinical Infectious Diseases* **2004**, *38* (6), 864-870.
(42) Matsuzaki, K. Why and how are peptide–lipid interactions utilized for self-defense? Magainins and tachyplesins as archetypes. *Biochimica et Biophysica Acta (BBA) - Biomembranes* **1999**, *1462*(1), 1-10.
(43) Hughes, M. P. The cellular zeta potential: cell electrophysiology beyond the membrane. *Integrative Biology* **2024**, *16*.
(44) Hancock, R. E. W.; Wiegand, I.; Hilpert, K. Agar and broth dilution methods to determine the minimal inhibitory concentration (MIC) of antimicrobial substances. *Nature Protocols* **2008**, *3*(2), 163-175.
(45) Vyhnalkova, R.; Eisenberg, A.; van de Ven, T. Bactericidal Block Copolymer Micelles. *Macromolecular Bioscience* **2011**, *11*(5), 639-651.
(46) Dhumal, D.; Maron, B.; Malach, E.; Lyu, Z.; Ding, L.; Marson, D.; Laurini, E.; Tintaru, A.; Ralahy, B.; Giorgio, S. Dynamic self-assembling supramolecular dendrimer nanosystems as potent antibacterial candidates against drug-resistant bacteria and biofilms. *Nanoscale* **2022**, *14*(26), 9286-9296.

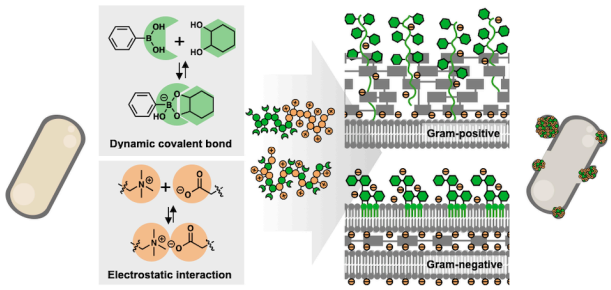

- *Chemical motifs to target bacterial cell surface*
- *Bactericidal activities*